Supplementary Information

Podoplanin maintains high endothelial venule integrity by interacting with platelet CLEC-2

Brett H. Herzog[1,2*], Jianxin Fu[1,3,4*], Stephen J. Wilson[5], Paul R. Hess[6], Aslihan Sen[6], J. Michael McDaniel[1], Yanfang Pan[1,2], Minjia Sheng[1], Tadayuki Yago[1], Robert Silasi-Mansat[1], Samuel McGee[1], Frauke May[7], Bernhard Nieswandt[7], Andrew J. Morris[8], Florea Lupu[1], Shaun R. Coughlin[5], Rodger P. McEver[1,2], Hong Chen[1,2], Mark L. Kahn[6], Lijun Xia[1,2,3,4]

[1]Cardiovascular Biology Research Program, Oklahoma Medical Research Foundation, Oklahoma City, Oklahoma 73104, USA. [2]Department of Biochemistry and Molecular Biology, University of Oklahoma Health Sciences Center, Oklahoma City, Oklahoma 73104, USA. [3]Jiangsu Institute of Hematology, The First Affiliated Hospital of Soochow University, Suzhou, Jiangsu 215006, China. [4]Key Laboratory of Thrombosis and Hemostasis of Ministry of Health, The First Affiliated Hospital of Soochow University, Suzhou, Jiangsu 215006, China. [5]Cardiovascular Research Institute, University of California, San Francisco, California 94158, USA. [6]Department of Medicine and Cardiovascular Institute, University of Pennsylvania, Philadelphia, Pennsylvania 19104, USA. [7]University Hospital Wurzburg and Rudolf Virchow Center, DFG-Research Center for Experimental Biomedicine, Wurzburg, Germany. [8]Division of Cardiovascular medicine, University of Kentucky and Veterans Affairs Medical Center, Lexington, Kentucky 40502, USA.

*These authors contributed equally to this study.

Correspondence:

Lijun Xia, Cardiovascular Biology Research Program, Oklahoma Medical Research Foundation, 825 N.E. 13th Street, Oklahoma City, OK 73104; Tel: (405) 271-7892; FAX: (405) 271-3137; e-mail: Lijun-Xia@omrf.org

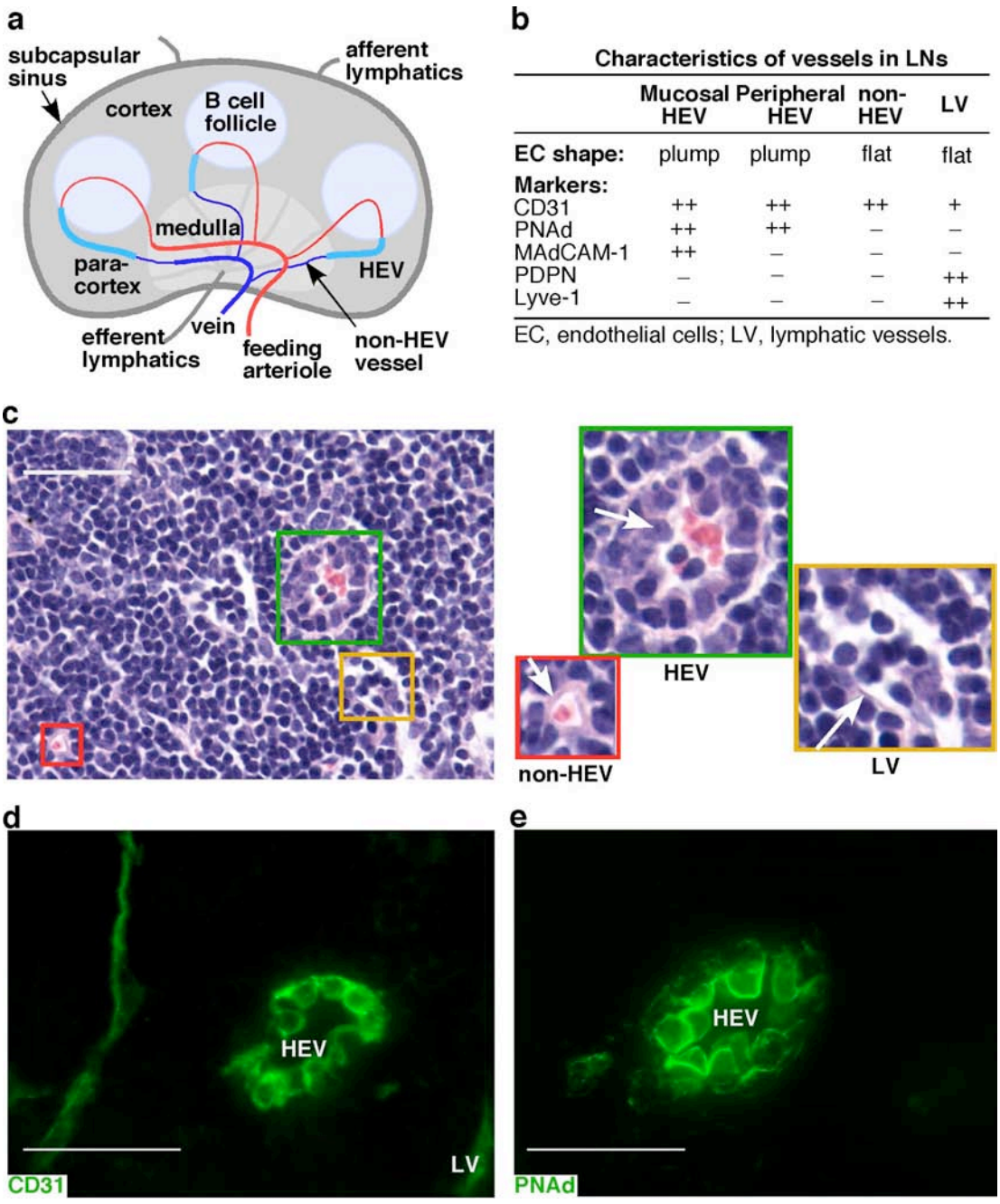

Supplementary Figure 1. Characteristics of different vessels in LNs. a, Diagram of an LN emphasising the vascular systems and HEVs. **b**, A summary of features of different vessels in LNs. PNAd, a specific marker for HEVs; MAdCAM-1, a specific marker for mucosal HEVs. **c**, An H&E-stained WT MLN section showing an HEV with its distinct cuboidal morphology, a flat-walled non-HEV vessel, and a flat thin-walled lymphatic vessel (LV) containing lymphocytes. Arrows indicate endothelial cells. **d** and **e**, Confocal images of WT MLN cryosections showing HEVs expressing a high level of CD31 (**d**) and PNAd (**e**). Scale bars, 50 μm.

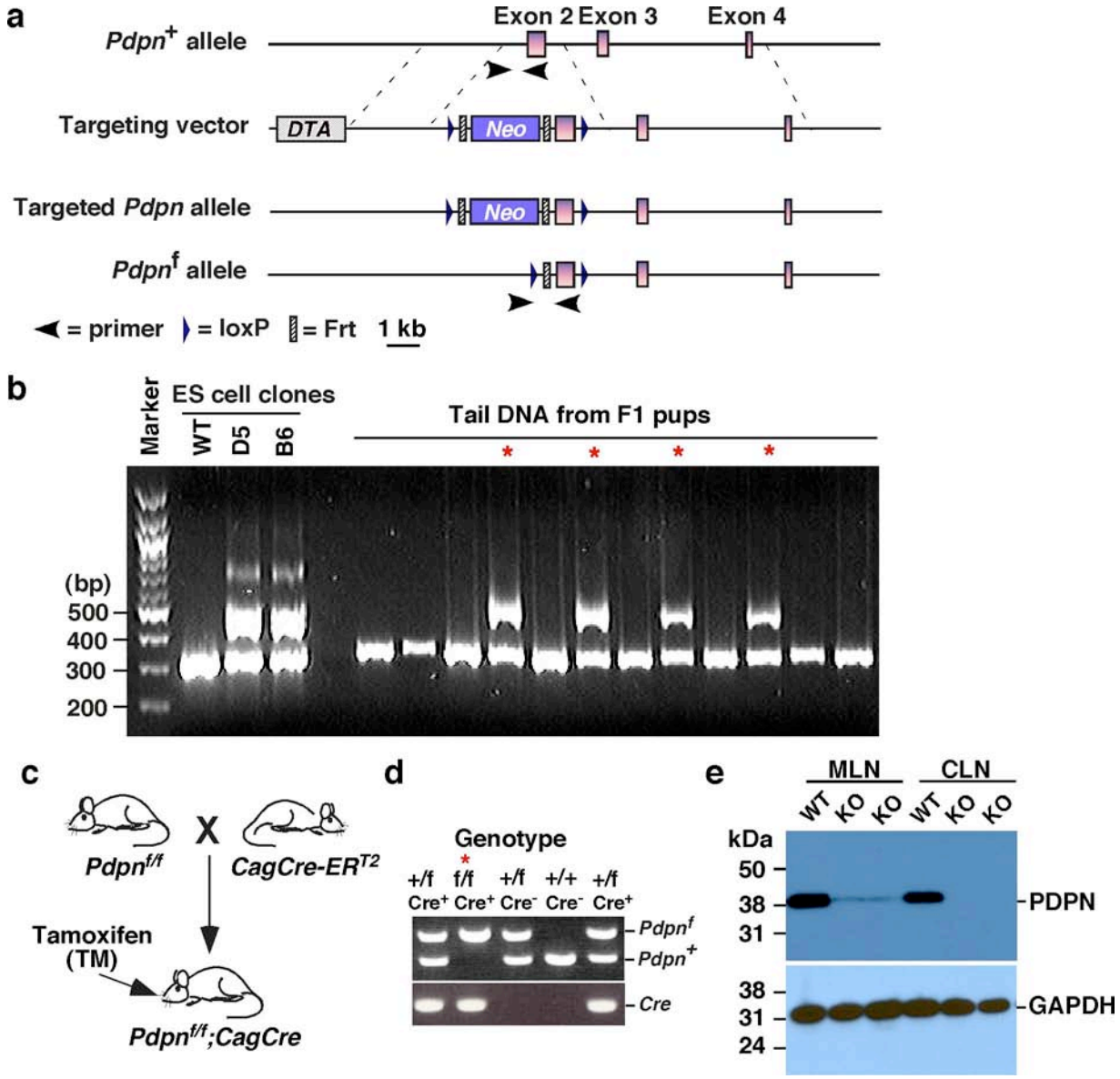

Supplementary Figure 2. Generation of *Pdpn* floxed and globally inducible PDPN-deficient mice. **a,** Gene targeting strategy for generating mice with a *Pdpn* allele flanked by loxP sites (*Pdpn*^{f}). **b,** PCR genotyping of F1 generation. WT and gene-targeted positive embryonic stem (ES) cell clones were used as controls. Asterisks indicate pups with germline transmission of the *Pdpn*^{f} allele. **c,** Breeding strategy to develop TM-inducible global PDPN-deficient mice, *Pdpn*$^{f/f}$*;CagCre* mice, by crossing *Pdpn*$^{f/f}$ mice with tamoxifen (TM)-inducible Cre-recombinase transgenic mice (CAG-Cre-ER^{T2} Tg) under control of a ubiquitous fusion promoter, CMV-early enhancer element/chicken beta-actin. **d,** PCR genotyping showing pups with the *Pdpn*$^{f/f}$ genotype (red asterisk). **e,** Immunoblot analysis of PDPN in MLNs and CLNs from P15 WT and *Pdpn*$^{f/f}$*;CagCre* mice 10 days after 20 μg tamoxifen was orally administered daily from P1 to P5. Glyceraldehyde-3-phosphate dehydrogenase (GAPDH) was used as a loading control. Three experiments showed similar results.

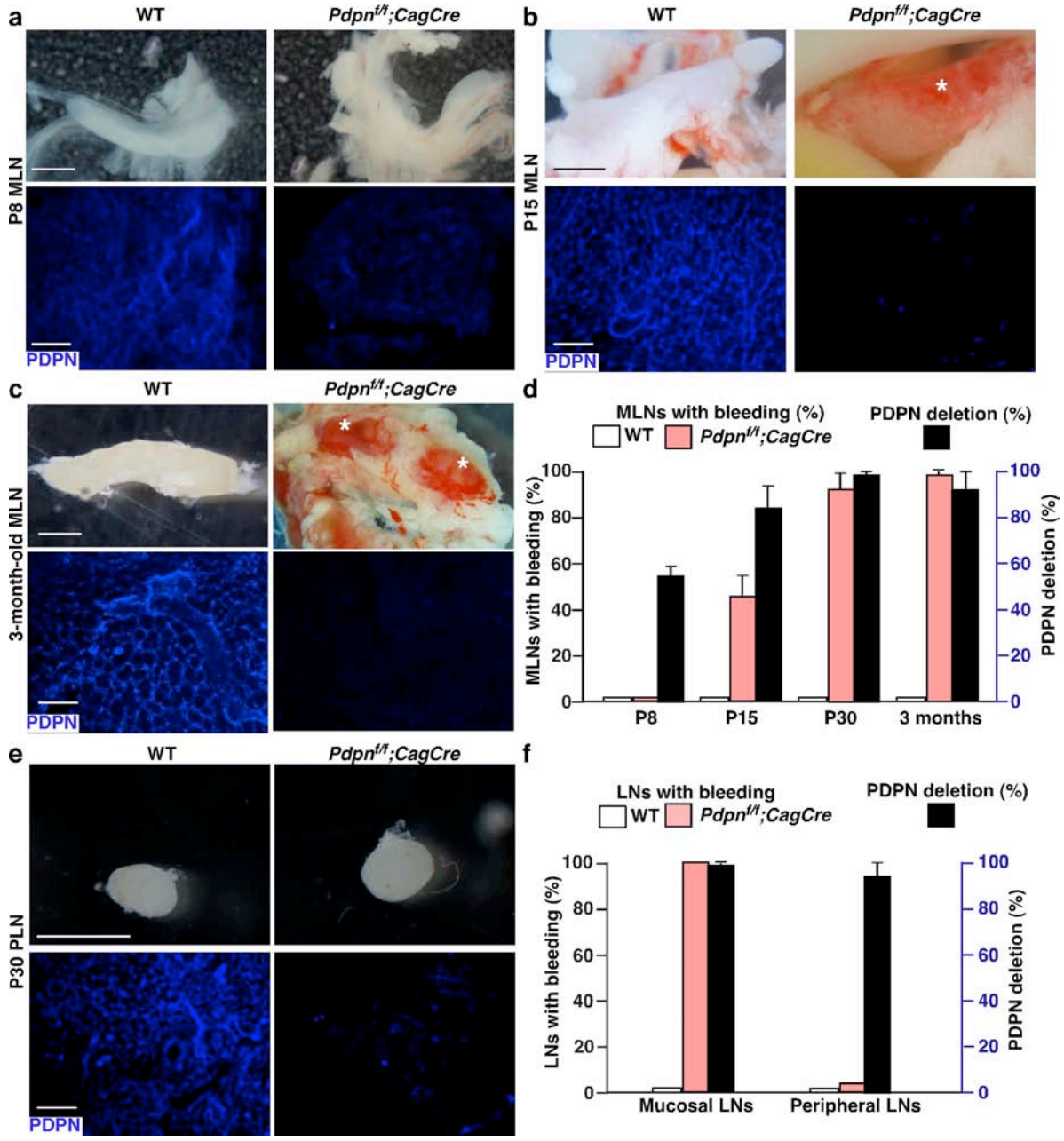

Supplementary Figure 3. Mucosal LN but not peripheral LN bleeding correlates with loss of PDPN after induced deletion. a-b, Representative gross images and confocal images of immunofluorescence staining for PDPN expression in MLNs after TM treatment (20 μg/ day from P1 to P5) from P8 mice (**a**) or P15 mice (**b**). Asterisk indicates bleeding. **c,** Representative gross images and confocal images for PDPN expression in MLNs from 3-month-old mice after TM treatment (1 mg/day from age 3 weeks for 1 week, and 1 mg/week thereafter). **d,** Frequency of MLN bleeding and percent of PDPN deletion at various times (mean ± s.d., n = 10 MLNs and 30 sections per group). **e,** Representative gross images and confocal images of PDPN staining in popliteal LNs (PLN), which represent peripheral LNs from 1-month-old (P30) mice after TM treatment. **f,** Frequency of MLN and peripheral (inguinal and popliteal) LN bleeding and percent of PDPN deletion. n = 34 LNs per group. Three cryosections per LN were analyzed. Scale bars, 2 mm (gross), 50 μm (confocal).

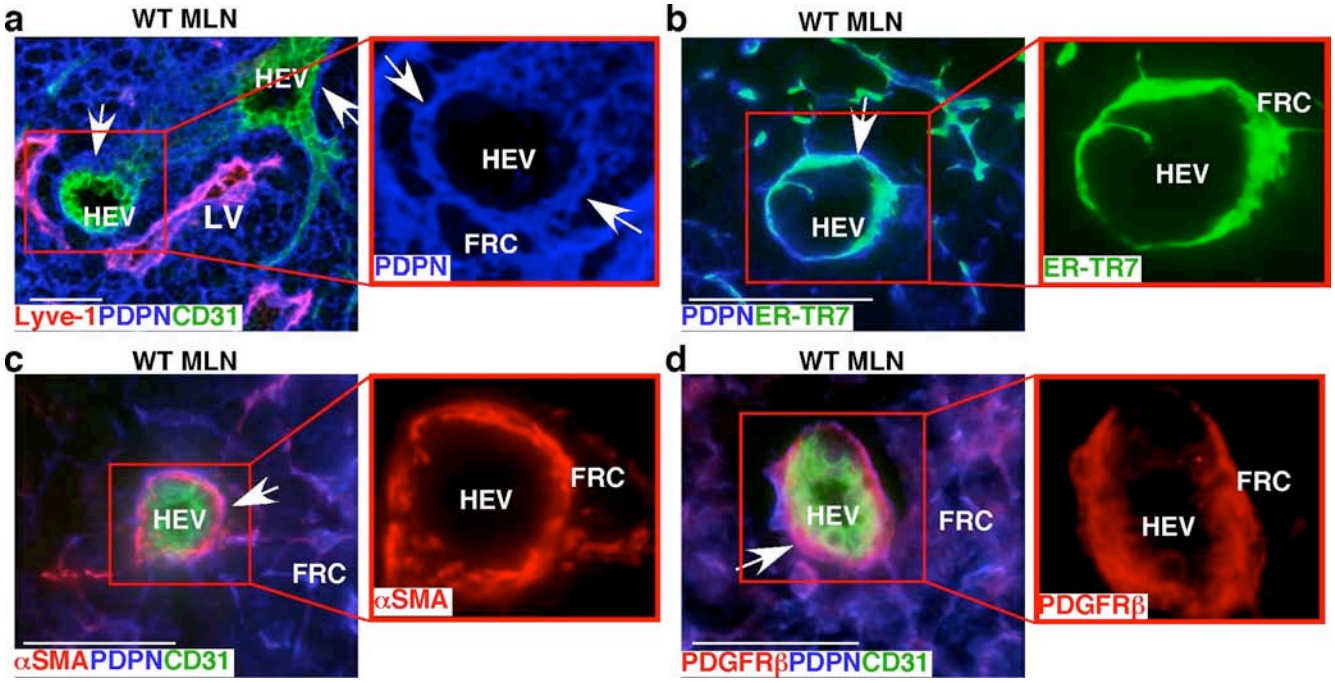

Supplementary Figure 4. PDPN is highly expressed on FRCs that surround HEVs. a-d, Confocal images of a 1-month-old WT MLN cryosection stained with antibodies to PDPN, Lyve-1, and CD31 (**a**); PDPN and ER-TR7 (**b**); PDPN, CD31, and αSMA (**c**); or PDGFRβ (**d**). ER-TR7, αSMA, and PDGFRβ are markers for FRCs. Arrows mark $PDPN^{+}$ FRCs. Scale bars, 50 μm.

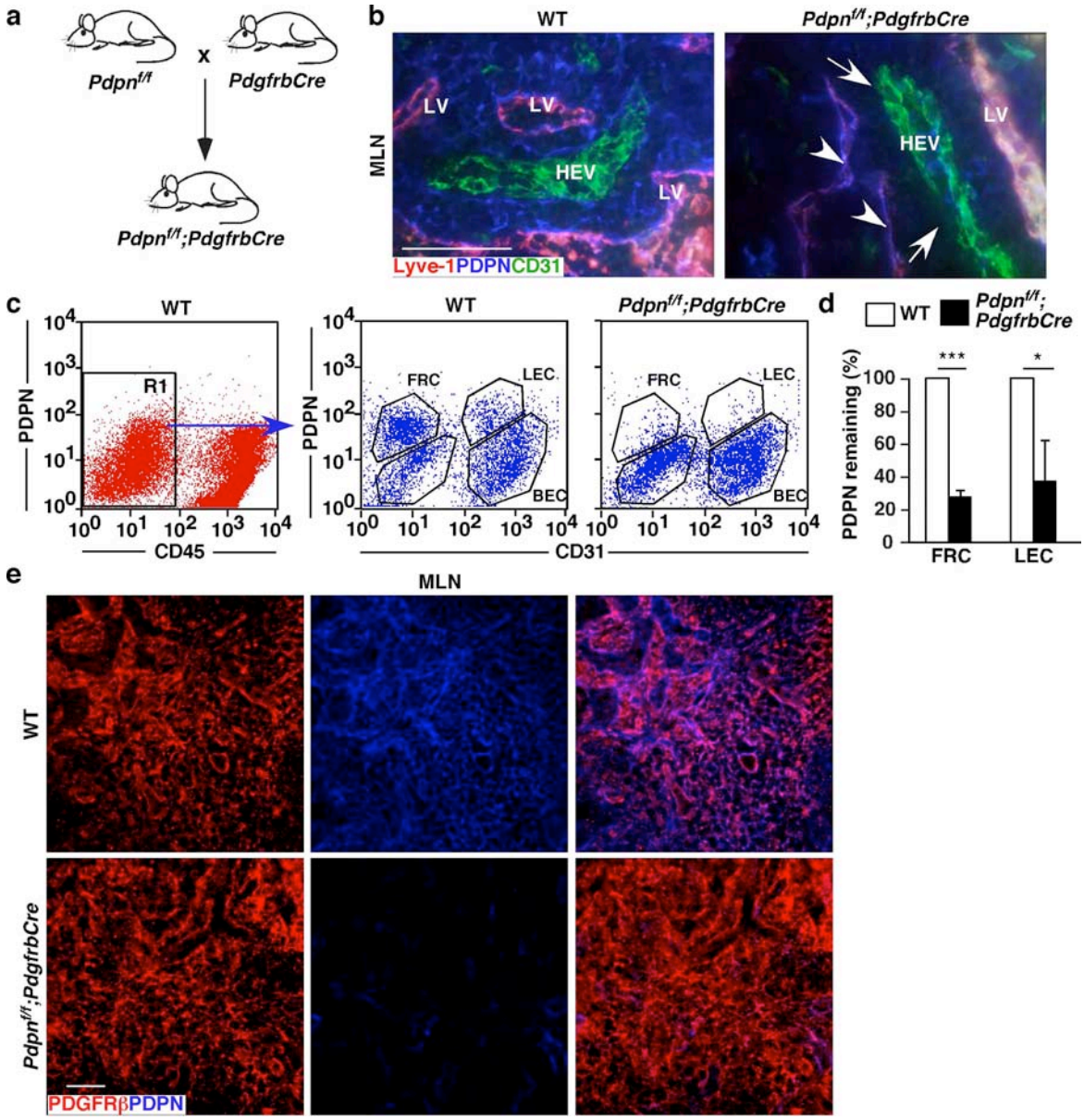

Supplementary Figure 5. Generation of mice lacking PDPN specifically in FRCs. a, Breeding strategy to develop mice lacking PDPN in PDGFRβ-expressing FRCs, *Pdpn$^{f/f}$;PdgfrbCre*, by crossing *Pdpn$^{f/f}$* mice with transgenic mice expressing Cre under control of the *Pdgfrb* promoter. **b,** Confocal images of PDPN, Lyve-1, and CD31 in MLNs showing considerably reduced levels of PDPN on FRCs around CD31$^+$ HEVs from *Pdpn$^{f/f}$;PdgfrbCre* mice (arrows) but not from WT mice. PDPN was also slightly reduced on lymphatic vessels (LV, arrowheads) of *Pdpn$^{f/f}$;PdgfrbCre* mice relative to that from WT mice. **c,** Flow cytometry analysis (gated on CD45$^-$ cells from LNs) shows that CD31$^-$ FRCs and CD31$^+$ LECs but not CD31$^-$ blood endothelial cells (BECs) of WT mice express PDPN. However, PDPN is reduced on FRCs and LECs of *Pdpn$^{f/f}$;PdgfrbCre* mice. **d,** Quantification of PDPN remaining on FRCs or LECs of LNs from *Pdpn$^{f/f}$;PdgfrbCre* mice compared with WT controls (mean ± s.d., $n = 6$ mice per group from three experiments). **e,** Confocal images of MLNs from WT or *Pdpn$^{f/f}$;PdgfrbCre* mice stained for PDPN and PDGFRβ showing that WT and *Pdpn$^{f/f}$;PdgfrbCre* had similar FRC morphological structures. Scale bars, 50 μm. *, $P < 0.05$; ***, $P < 0.001$.

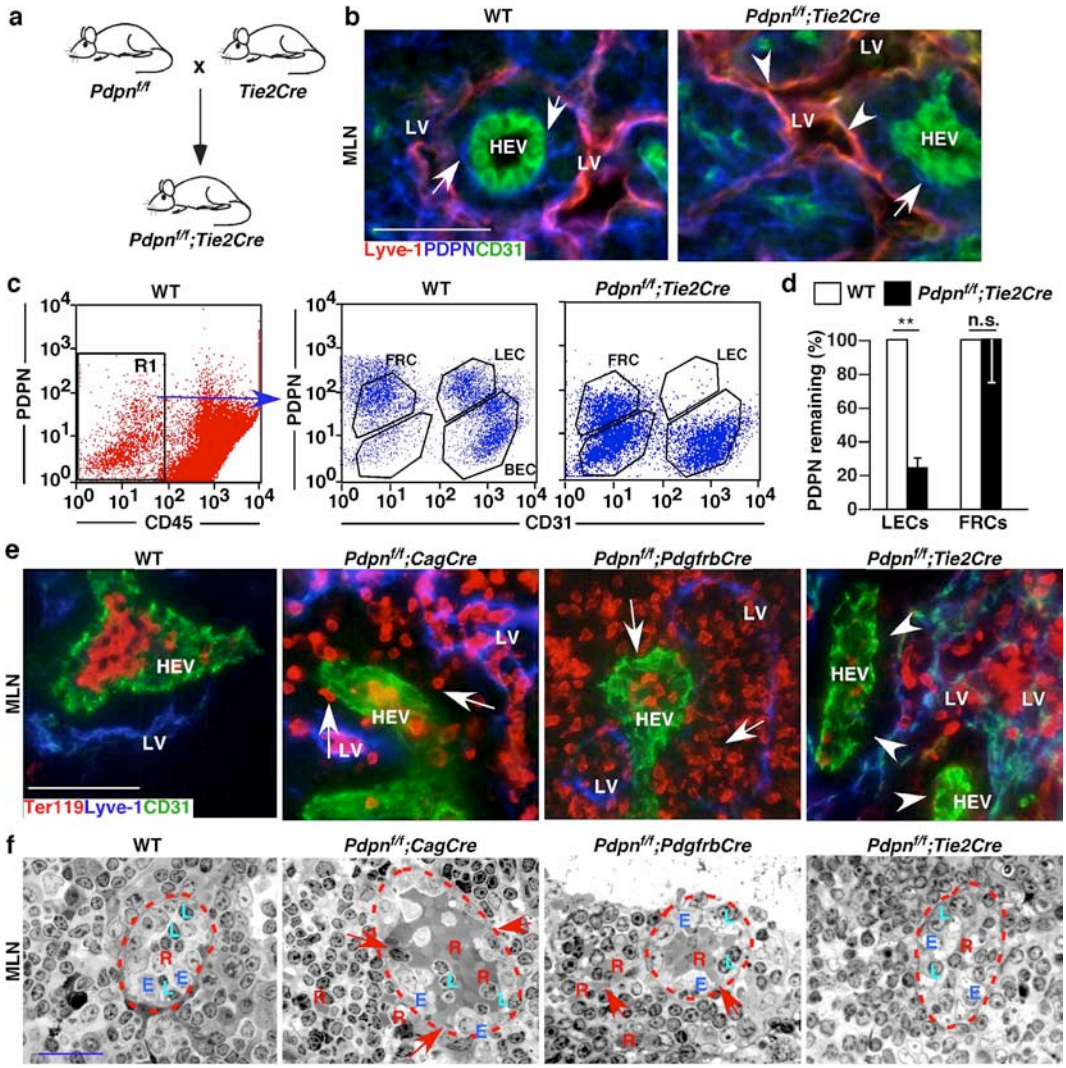

Supplementary Figure 6. Generation of mice lacking PDPN specifically in endothelial cells including LECs. a, Breeding strategy to develop mice lacking PDPN in endothelial cells, *Pdpn$^{f/f}$;Tie2Cre* mice, by crossing *Pdpn$^{f/f}$* mice with Tie2Cre transgenic mice. **b,** Confocal images of PDPN, Lyve-1, and CD31 staining in MLNs from WT and *Pdpn$^{f/f}$;Tie2Cre* mice. Arrows indicate PDPN^{+} FRCs surrounding CD31^{+} HEVs. Arrowheads indicate lymphatic vessels (LV) with PDPN deletion. **c,** Flow cytometry analysis (gated on CD45^{-} cells from LNs) shows that PDPN is reduced on LECs but not FRCs of *Pdpn$^{f/f}$;Tie2Cre* mice. **d,** Quantification of PDPN remaining on LECs and FRCs of LNs from *Pdpn$^{f/f}$;Tie2Cre* mice compared with WT controls (mean ± s.d. $n = 6$ mice per group from three experiments). **e,** Confocal images of cryosections of MLNs from mice lacking PDPN in different cell types. Arrows indicate Ter119^{+} RBCs extravasated outside HEVs in *Pdpn$^{f/f}$;CagCre* and *Pdpn$^{f/f}$;PdgfrbCre* mice. Arrowheads show no extravasated RBCs around HEVs in *Pdpn$^{f/f}$;Tie2Cre* mice. **f,** Morphological analyses of HEVs in MLNs from mice lacking PDPN in different cell types based on toluidine blue–stained semi-thin sections (~300 nm, grayscale). Red arrows indicate RBCs (R) extravasated or in gaps between high endothelial cells (E). L, leukocytes. Dashed lines indicate HEVs. **e, f,** Six mice per group were analyzed in two separate experiments. Scale bars, 50 μm (confocal), 25 μm (semi-thin). **, $P < 0.01$; n.s., no significance.

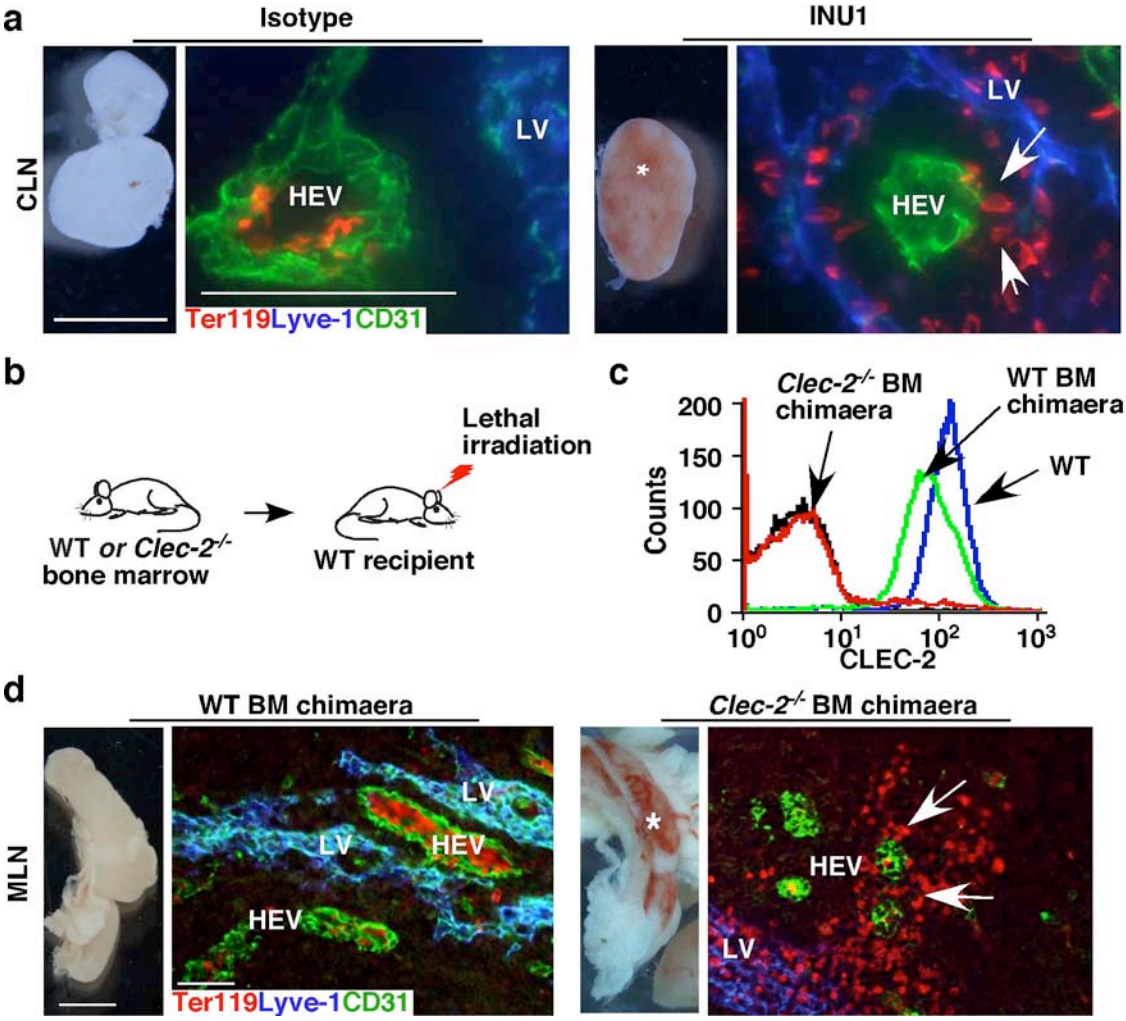

Supplementary Figure 7. Postnatal loss of CLEC-2 function causes bleeding in LNs. a, Gross images and confocal analysis of P15 CLNs from WT mice treated with the mAb INU1, which depletes CLEC-2 in vivo, or isotype control Rat IgG1κ. Asterisk indicates bleeding. Arrows indicate Ter119$^+$ RBCs around an HEV. n = 20 LNs per group from four experiments. **b,** Diagram depicting generation of WT > WT and *Clec-2*$^{-/-}$ > WT bone marrow irradiation chimaeras (WT or *Clec-2*$^{-/-}$ BM chimaera, respectively). **c,** Flow cytometry analysis of CLEC-2 expression on platelets from peripheral blood 12 weeks after bone marrow transplantation (n = 8 mice/group). **d,** Gross images and confocal analysis of MLNs from WT and *Clec-2*$^{-/-}$ BM chimaera mice. Asterisk indicates bleeding. Arrows indicate Ter119$^+$ RBCs outside HEVs. Data represent at least three experiments. Scale bars, 2 mm (gross), 50 μm (confocal).

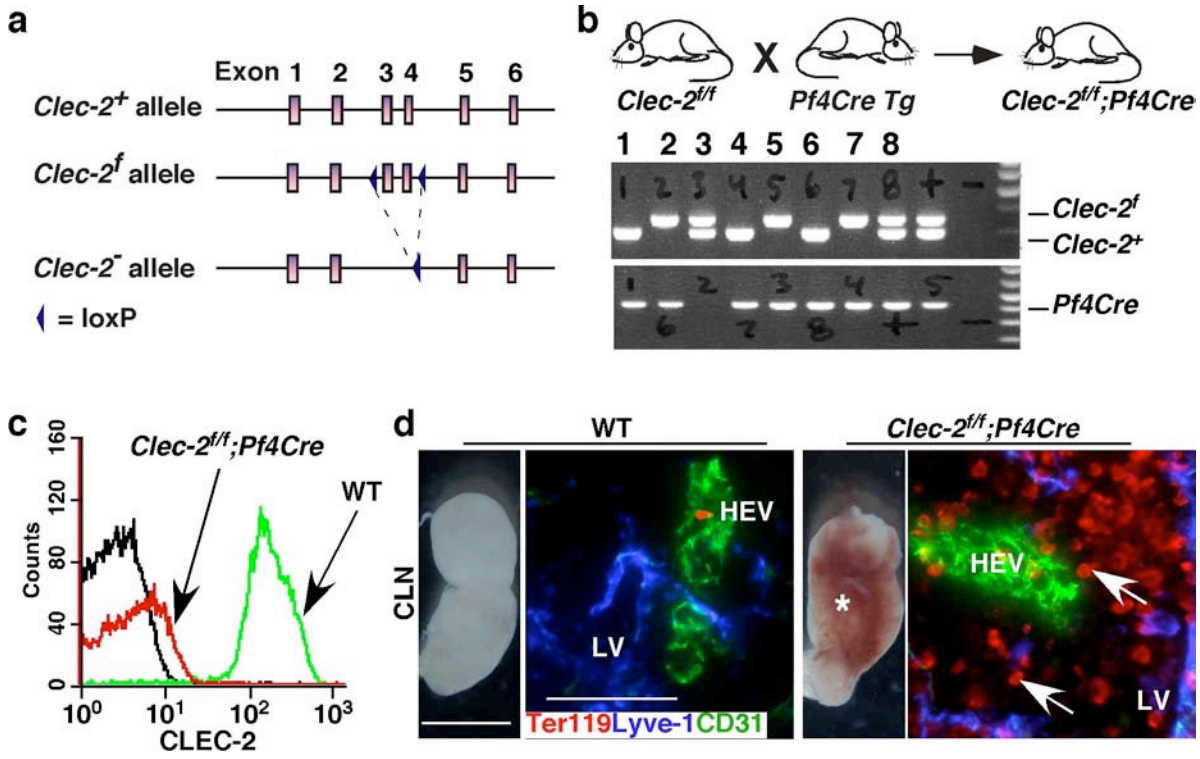

Supplementary Figure 8. Mice lacking CLEC-2 specifically on platelets have spontaneous bleeding in LNs. a, Gene targeting strategy for generating mice with a *Clec-2* allele flanked by loxP sites (*Clec-2*^{f}). **b,** Breeding strategy to develop platelet-specific deletion of CLEC-2 by crossing *Clec-2*$^{f/f}$ mice with mice expressing Cre-recombinase under the control of the megakaryocyte-specific promoter *Pf4* (Pf4Cre Tg). PCR genotyping showing pups with the *Clec-2*$^{f/f}$*;Pf4Cre* genotype (#5 and #7). **c,** Flow cytometry analysis of CLEC-2 expression on platelets from peripheral blood of 1-month-old WT and *Clec-2*$^{f/f}$*;Pf4Cre* mice. **d,** Gross morphology and confocal images of CLNs from 1-month-old WT and *Clec-2*$^{f/f}$*;Pf4Cre* mice. Asterisk indicates bleeding. Arrows indicate extravasated Ter119^{+} RBCs. Data represents eight mice per group from two experiments. Scale bars, 2 mm (gross), 50 μm (confocal).

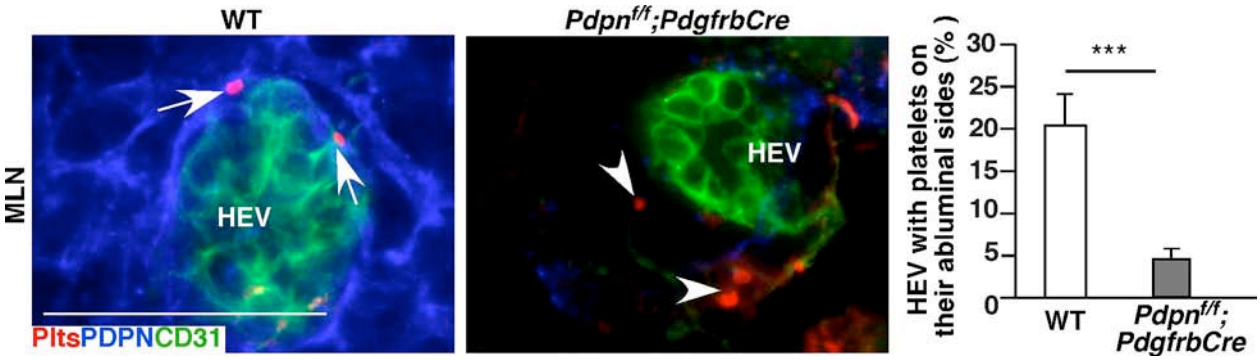

Supplementary Figure 9. Loss of FRC PDPN decreases abluminal platelet localization around HEVs. Confocal images of MLN cryosections stained with antibodies to CD31, platelets, and PDPN. Arrows indicate platelets on the abluminal side of HEVs. Arrowheads indicate platelets that are not closely associated with HEVs. Bar graph on the right represents percentage of HEVs with platelets on their abluminal side (mean ± s.d., 250 HEVs/mouse (n = 3)). Scale bar, 50 μm.

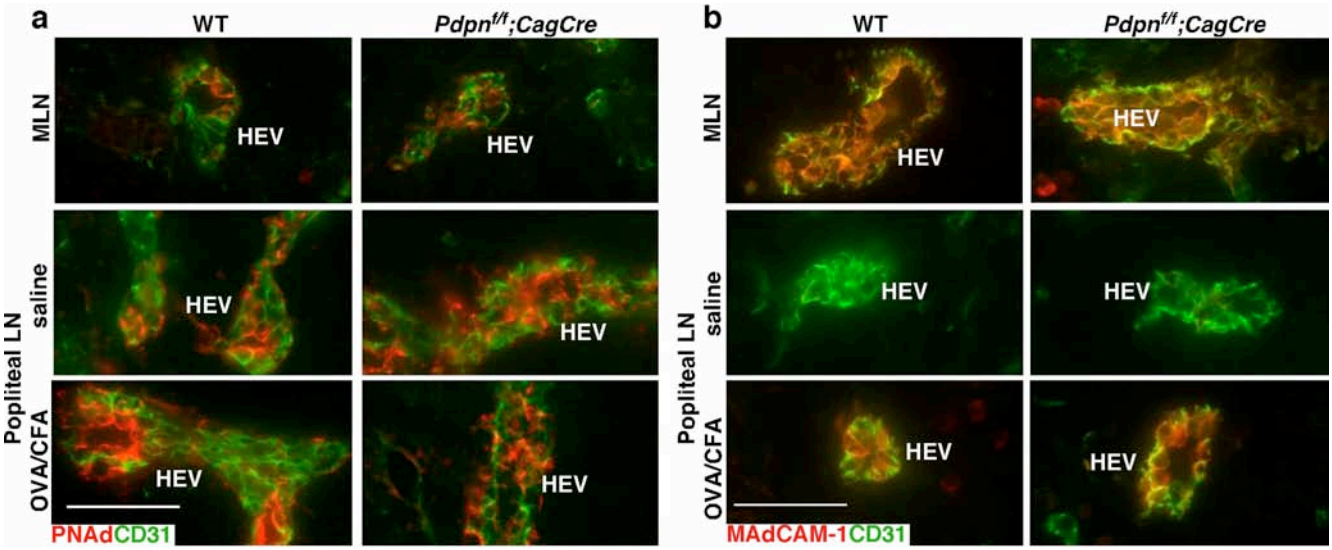

Supplementary Figure 10. Mucosal LNs share similar molecular signatures with immunised "*reactive*" peripheral LNs. a-b, Confocal analyses of cryosections of MLNs or popliteal LNs with or without OVA/CFA challenge from 1-month-old WT and *Pdpn$^{f/f}$;CagCre* mice after staining with antibodies to CD31 and PNAd (**a)** or MAdCAM-1 (**b**), a mucosal LN-specific HEV marker. Data represents two experiments in which 150 HEVs/group (n = 3) were analyzed. Scale bars, 50 μm.

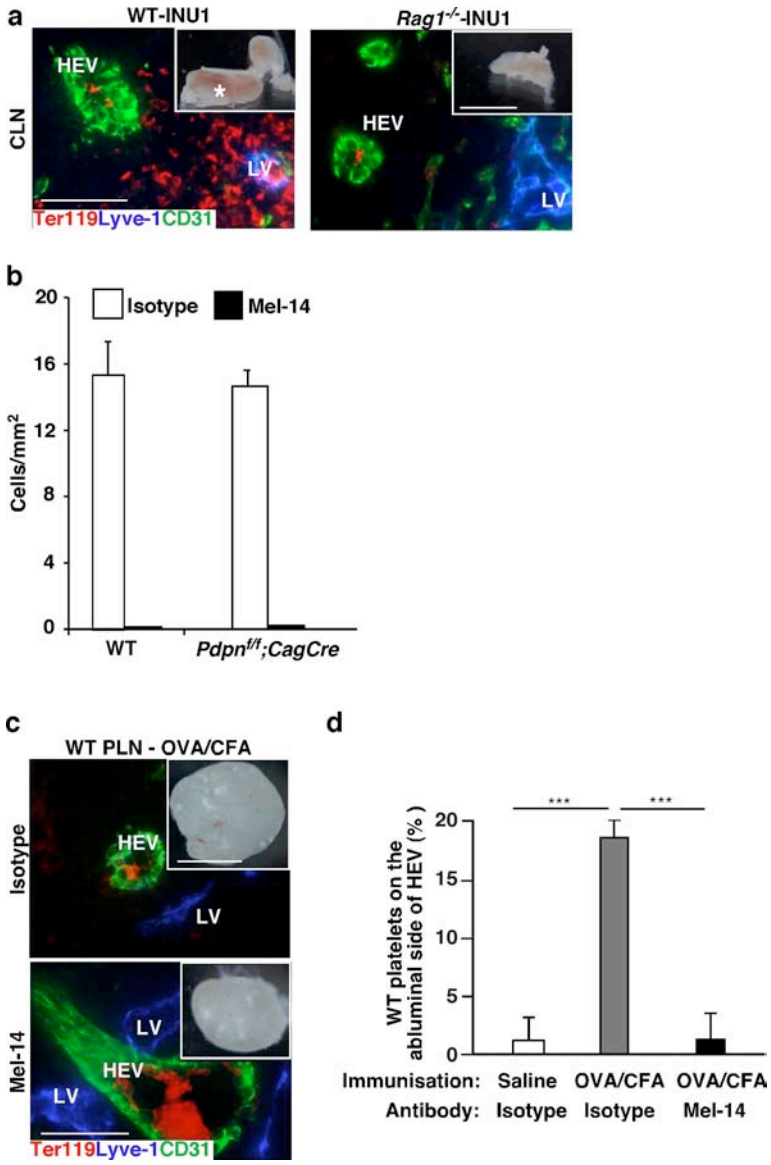

Supplementary Figure 11. Blocking lymphocyte trafficking through HEVs ameliorates HEV bleeding. a, Gross morphology (insets) and confocal images of CLNs from 2-week-old WT and *Rag1*$^{-/-}$ mice treated with mAb INU1 that depletes CLEC-2 in vivo. Asterisk indicates bleeding. $n = 6$ LNs per group. **b**, Frequency of peripheral leukocytes rolling on 6-sulpho-sLe^{x}, which is the functional epitope of L-selectin ligands, coated surfaces under flow conditions in an in vitro flow-chamber assay to demonstrate the effectiveness of in vivo blockade of L-selectin function using anti-L-selectin (Mel-14). The leukocytes were isolated from mice after intravenous injections with anti-L-selectin (Mel-14) or isotype control rat IgG (mean ± s.d., $n = 4$ mice from two experiments). **c,** Gross morphology (insets) and confocal images of draining popliteal LNs (PLN) from 1-month-old WT mice one week after OVA/CFA challenge and injections with Mel-14, an anti-L-selectin-blocking mAb, or isotype control rat IgG. **d,** Percentage of HEVs with platelets on their abluminal surface in PLNs of WT mice without challenge, with OVA/CFA challenge and an isotype control rat IgG, and with OVA/CFA challenge and Mel-14 (mean ± s.d., 150 HEVs/group ($n = 4$)). Scale bars, 2 mm (gross), 50 μm (confocal).

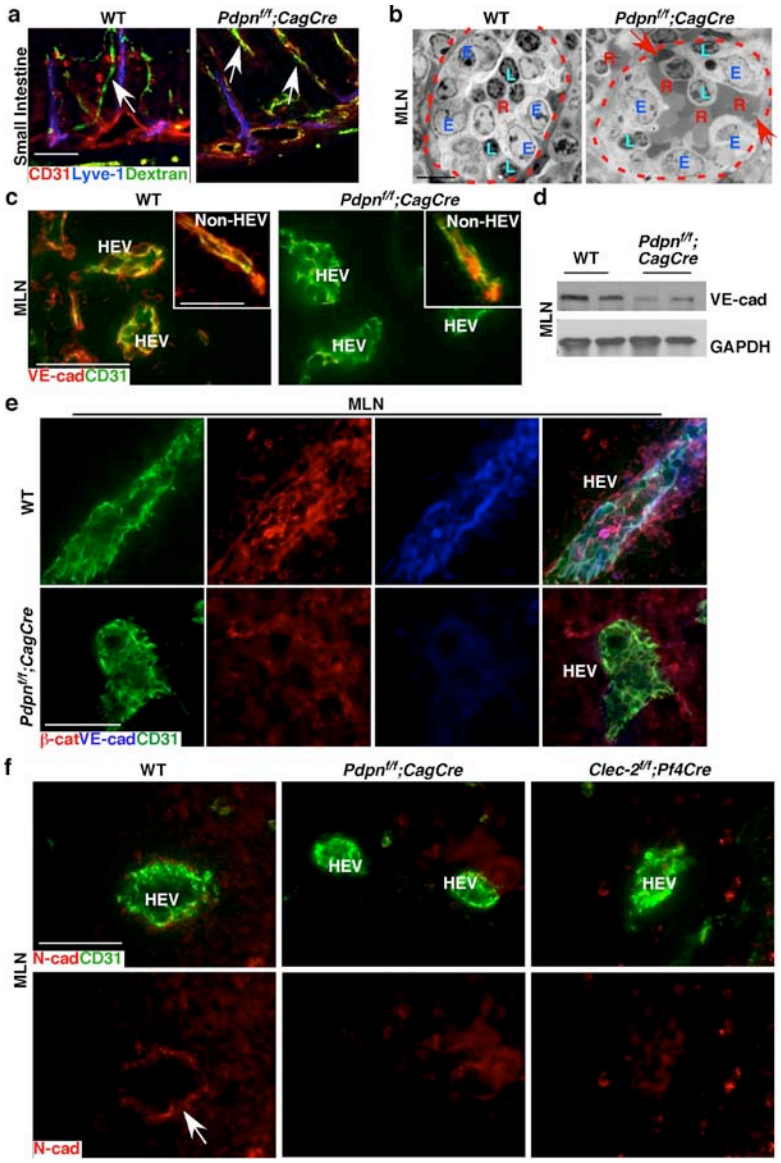

Supplementary Figure 12. Altered HEV adherens junctions are found in *Pdpn$^{f/f}$;CagCre* mice. **a,** Confocal images of intravenously injected FITC-dextran (2,000 kDa) in the small intestine showing no leakage of FITC-dextran in intestinal blood vessels of P15 PDPN-deficient mice (arrows). **b,** Resin-embedded semi-thin MLN sections (~300 nm) stained with toluidine blue and converted to grayscale. Red arrows indicate RBCs (R) between gaps of high endothelial cells (E). L, leukocytes. Red dashed lines outline HEVs. **c,** Merged confocal images from Fig. 3d showing CD31 and VE-cad staining in HEVs of P8 MLNs. Insets show CD31 and VE-cad staining in non-HEV blood vessels. **d,** Immunoblot analysis of VE-cad in MLNs of 1-month-old WT and *Pdpn$^{f/f}$;CagCre* mice (n = 6 mice/group). GAPDH used as a loading control. **e,** Confocal images of cryosections of MLNs from WT and *Pdpn$^{f/f}$;CagCre* mice stained with antibodies against CD31, β-catenin (β-cat), and VE-cad. **f,** Confocal images of cryosections of MLNs from WT and *Pdpn$^{f/f}$;CagCre* mice stained with antibodies against CD31 and N-cadherin (N-cad, arrow). **e, f,** Data represents two experiments in which 150 HEVs/group (n = 3) were analyzed. Scale bars, 50 μm (confocal) and 25 μm (insets), 10 μm (semi-thin).

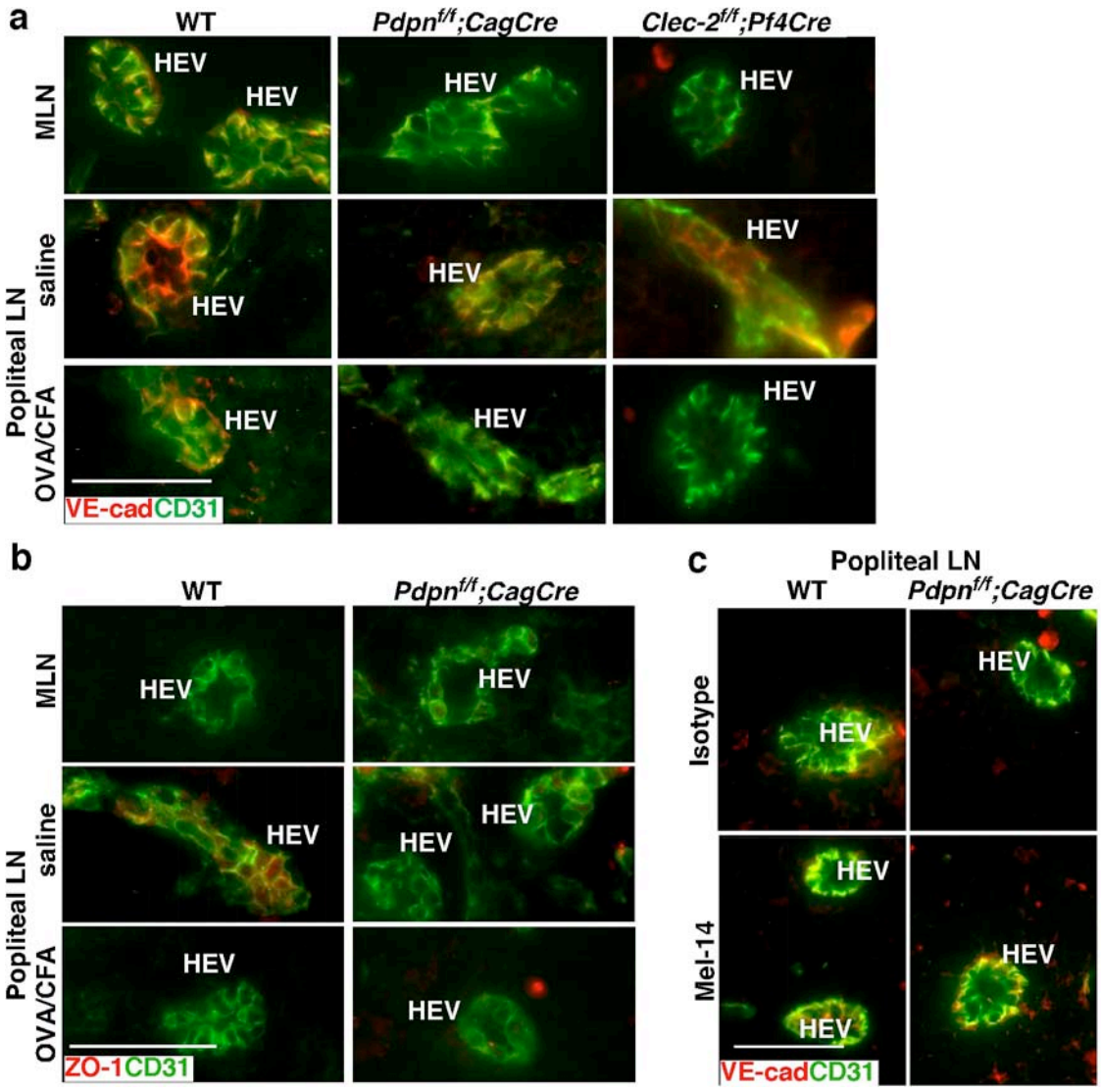

Supplementary Figure 13. The molecular features of mucosal HEV junctions resemble those of "*reactive*" peripheral HEVs. a, Confocal analyses of cryosections of MLNs or draining popliteal LNs with or without OVA/CFA challenge from 1-month-old WT, *Pdpn$^{f/f}$;CagCre*, and *Clec-2$^{f/f}$;Pf4Cre* mice after staining with antibodies to CD31 and VE-cad. **b,** Confocal analyses of cryosections of MLNs or draining popliteal LNs with or without OVA/CFA challenge from 1-month-old WT and *Pdpn$^{f/f}$;CagCre* mice after staining with antibodies to CD31 and ZO-1. **c,** Confocal images of draining popliteal LNs with OVA/CFA challenge from 1-month-old WT and *Pdpn$^{f/f}$;CagCre* mice treated with an anti-L-selectin antibody (Mel-14) or an IgG control antibody and stained for CD31 and VE-cad. Data represents at least 100 HEVs per group from three experiments (n = 4) for each panel. Scale bars, 50 μm.

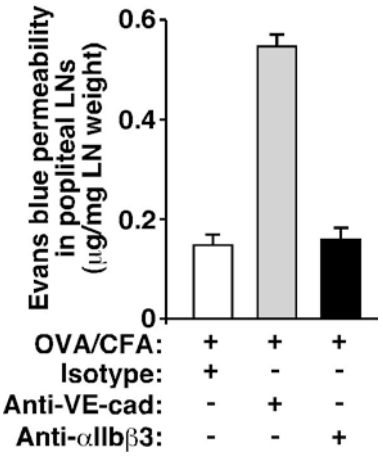

Supplementary Figure 14. Blocking VE-cad, but not platelet αIIbβ3**, increases LN permeability.** Comparison of Evans blue permeability between immune challenged popliteal LNs of 1-month-old WT mice after injections of 11D4.1, an anti-VE-cad blocking monoclonal antibody; JON/A, an anti-αIIbβ3 blocking mAb (inhibiting platelet aggregation), or an isotype control rat IgG. *n* = 4 mice per group.

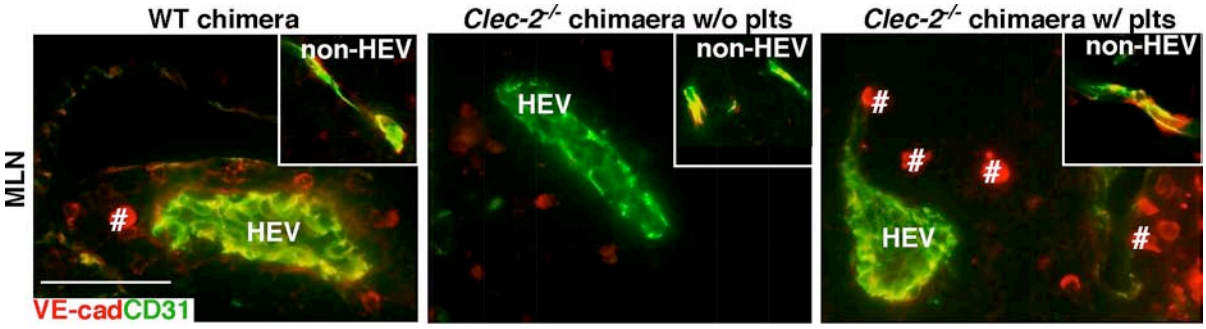

Supplementary Figure 15. Normalization of VE-cad expression on HEVs from CLEC-2 deficient mice after WT platelet transfusion. Merged confocal images from Fig. 3f showing CD31 and VE-cad staining in HEVs and non-HEVs (insets) in WT BM chimaeras (WT chimaera), and *Clec2*$^{-/-}$ BM chimaeras (*Clec2*$^{-/-}$ chimaeras) without or with previous injections (i.v.) with WT plts. # marks non-specific staining. Scale bar, 50 μm.

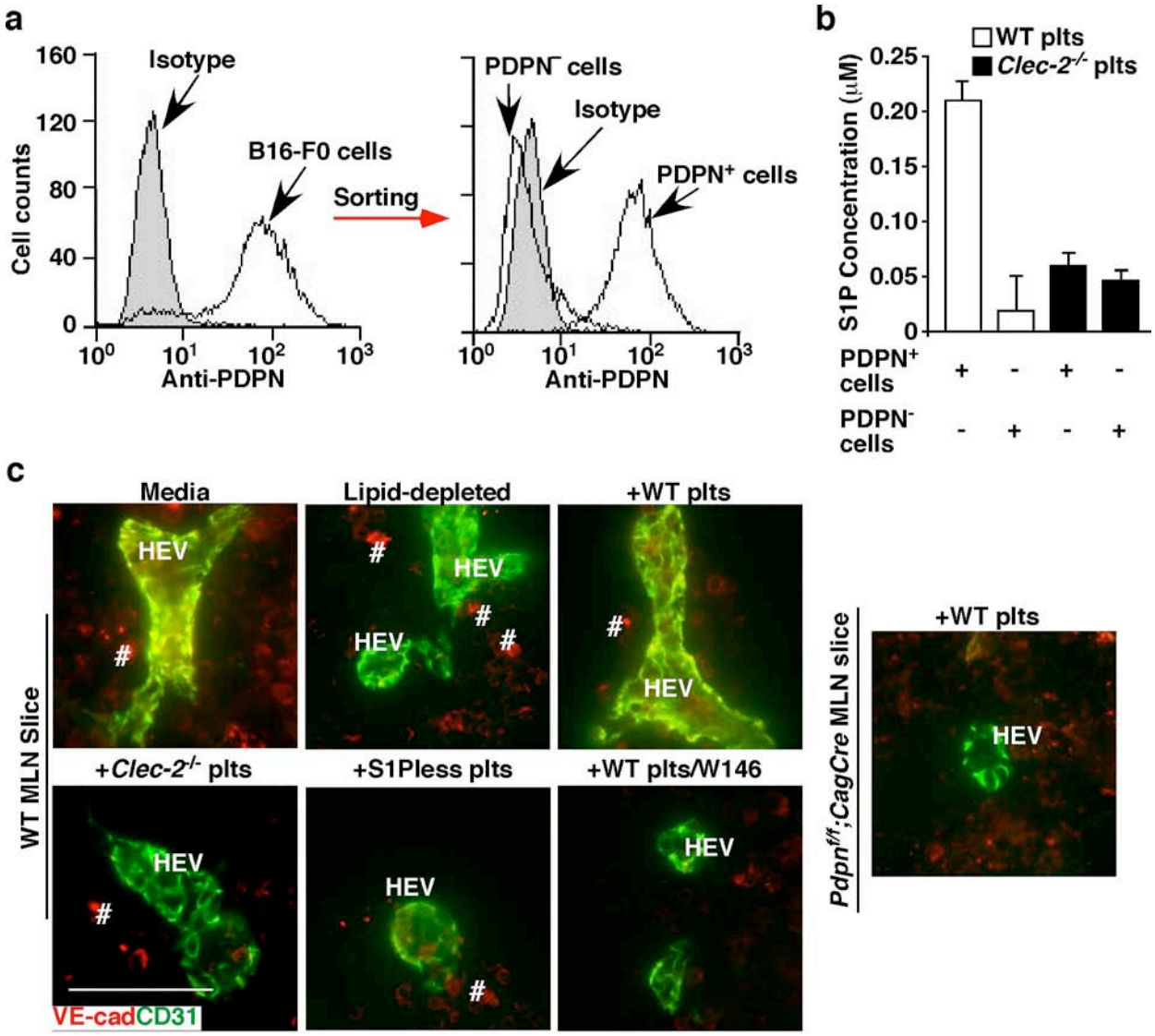

Supplementary Figure 16. Activation of CLEC-2 by PDPN induces S1P release from platelets, which maintains HEV VE-cad. a, Flow cytometry analysis of PDPN expression in B16-F0 melanoma cells before (left) and after (right) cell sorting for PDPN expression. Syrian hamster IgG was used as an isotype control (grey shaded histograms). **b,** Mass spectrometry measurements of S1P concentrations in supernatants of WT and *Clec-2*$^{-/-}$ platelets after incubation with PDPN^{+} or PDPN^{-} melanoma cells (mean from 2 samples per group). **c,** Merged images from Fig. 4b showing CD31 and VE-cad staining of HEVs from WT LN slices incubated for 1.5 hrs with DMEM and normal FBS (media), DMEM and lipid-depleted FBS (lipid-depleted), lipid-depleted and WT platelets (+WT plts), lipid-depleted and *Clec-2*$^{-/-}$ platelets (+*Clec-2*$^{-/-}$ plts), lipid-depleted and S1Pless platelets (+S1Pless plts), or lipid-depleted and WT plts plus S1PR1 antagonist W146 (+WT plts /W146). *Pdpn*$^{f/f}$*;CagCre* LN slices incubated with lipid-depleted and WT platelets (+WT plts) were controls. 100 HEVs analyzed per condition. # indicates non-specific staining also observed in negative controls. Scale bars, 50 μm.

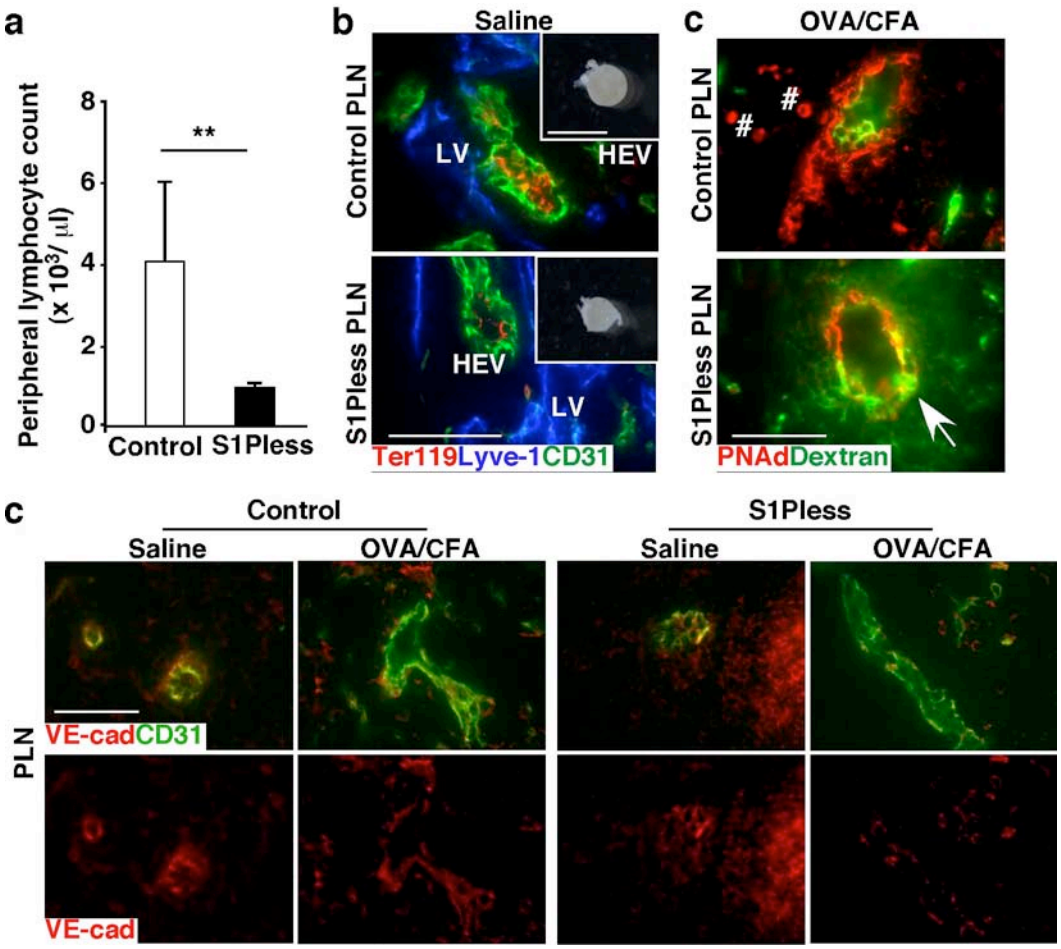

Supplementary Figure 17. S1P maintains HEV integrity. a, Peripheral lymphocyte count from whole blood of S1Pless and control mice (mean ± s.d., $n = 8$ mice). **b,** Gross morphology (insets) and confocal images of draining S1Pless or littermate control popliteal LNs (PLN). LV, lymphatic vessel (Lyve-1$^+$); HEV (CD31$^+$). **c,** Confocal images of PLN HEVs from S1Pless mice or littermate controls after intravenous FITC-dextran injection. Arrows indicate vascular leak of FITC-dextran. # indicate non-specific staining. **d**, Confocal images of draining PLN from WT and S1Pless mice with or without OVA/CFA challenge stained with antibodies against CD31 and VE-cad. $n = 150$ HEVs/group from three experiments ($n = 4$). Scale bars, 50 μm. **, $P < 0.01$.

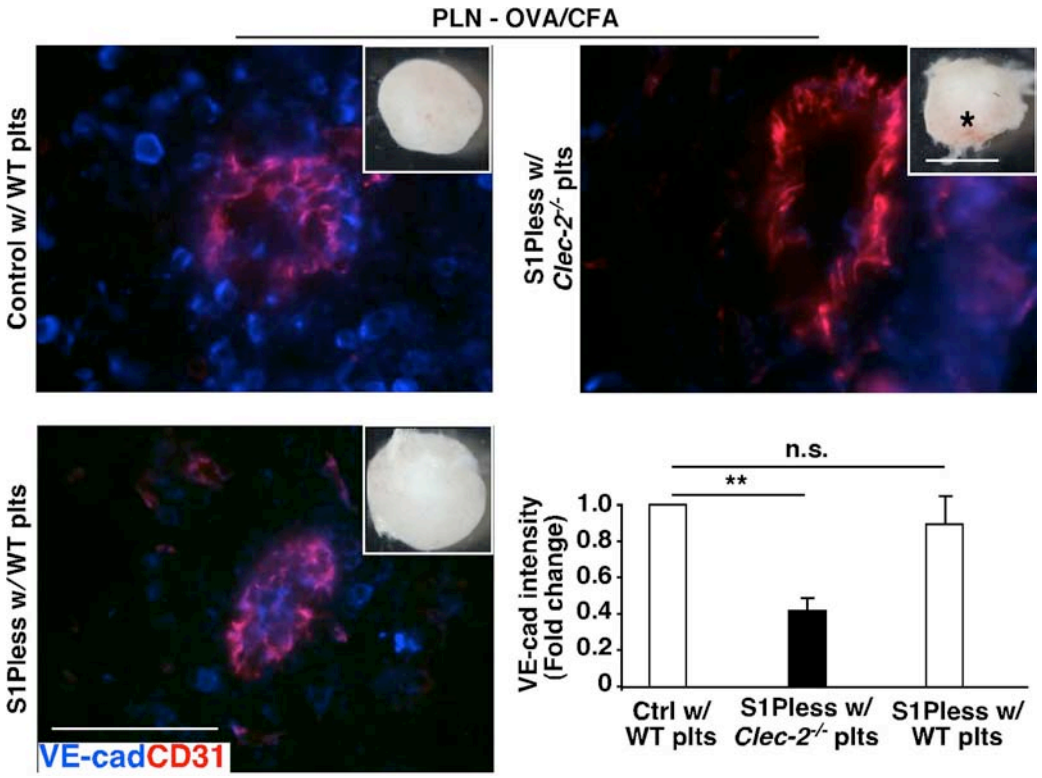

Supplementary Figure 18. Platelet S1P promotes VE-cad expression on HEVs in vivo. Gross morphology (insets) and confocal images of CD31 and VE-cad staining of HEVs from S1Pless mice or littermate control (Ctrl) popliteal LNs (PLN). n = 50 HEVs analyzed per condition. Graphs represent ratios of VE-cad intensities on HEVs relative to control mice transfused with WT platelets (plts) (mean ± s.d., n = 3 per group). Asterisks indicates bleeding. Scale bars, 2 mm (gross images), 50 μm (confocal images). **, $P < 0.01$; n.s., no significance.